Available online at www.sciencedirect.com
SCIENCE DIRECT®
C. R. Physique 4 (2003) 1035–1045
COMPTES RENDUS PHYSIQUE

Carbon nanotubes: state of the art and applications/Les nanotubes de carbone : état de l'art et applications

Phonons in alkali-doped single-wall carbon nanotube bundles

Jean-Louis Sauvajol [a], N. Bendiab [a], Eric Anglaret [a], Pierre Petit [b]

[a] *Groupe de dynamique des phases condensées (UMR CNRS 5581),Université Montpellier II, 34095 Montpellier cedex 5, France*
[b] *Institut Charles Sadron, 6, rue Boussingault, 67000 Strasbourg cedex, France*

Presented by Guy Laval

Abstract

We review Raman spectroscopy of alkali-doped single-wall carbon nanotube bundles. These results are correlated to resistivity and optical absorption measurements performed on the same samples. In this review we focus on the behavior of the high-frequency tangential modes upon doping. A doping-induced upshift of the tangential modes, concomitant to a loss of absorption bands in the optical spectra and to a monotonic decrease of the resistivity, is stated. The Raman response measured on the first plateau of the resistivity curve is featured by a symmetric single component upshifted with respect to pristine sample. This response is assigned to the Raman signature of a specific doped phase, labelled phase I. By contrast the Raman response of the saturated phase, associated to a second plateau in the resistance curve, is featured by a Breit–Wigner–Fano component downshifted with respect to the pristine sample. ***To cite this article: J.-L. Sauvajol et al., C. R. Physique 4 (2003).***

Résumé

Phonons dans les phases dopées aux alcalins des nanotubes de carbone monofeuillets. Dans cet article nous faisons une revue des résultats de spectroscopie Raman obtenus sur les phases dopées des faisceaux de nanotubes de carbone monofeuillets. Nous mettons en relation les évolutions des spectres Raman sous l'effet du dopage avec celles de la résistivité et de l'absorption optique mesurées sur les mêmes échantillons. Nous nous focalisons sur les changements du profil des modes tangentiels induits par le dopage. Dans un premier temps, un durcissement de ces modes, concomitant avec la disparition progressive des bandes d'absorption optique et la chute de la résistivité, est clairement établi. La réponse Raman associée à un premier plateau de résistivité se caractérise par un mode unique symétrique déplacé vers les hautes fréquences par rapport à sa position de départ. Cette réponse est considérée comme la signature Raman d'une phase dopée spécifique nommée phase I. À l'opposé, la réponse Raman de la phase dopée à saturation (second plateau de résistivité) se caractérise par une forme de raie de type Breit–Wigner–Fano déplacée vers les basses fréquences par rapport à la fréquence du mode tangentiel dominant des nanotubes non dopés. ***Pour citer cet article : J.-L. Sauvajol et al., C. R. Physique 4 (2003).***

Keywords: Carbon nanotube bundles; Raman spectroscopy

Mots-clés : Nanotubes de carbone monofeuillets ; spectroscopie Raman

E-mail addresses: sauva@gdpc.univ-montp2.fr (J.-L. Sauvajol), petit@ics.u-strasbg.fr (P. Petit).

1631-0705/$ – see front matter
doi:10.1016/S1631-0705(03)00099-9

1. Introduction

Intercalation compounds of carbon materials are of considerable interest. Intercalation of C_{60} fullerite with alkali metals led to the discovery of superconductivity with transition temperature surpassed only by the high-T_c oxides [1]. Because of their specific structures [2], single wall carbon nanotube (SWNT) bundles are an interesting intercalation host. It was demonstrated that SWNT bundles can form synthetic metals by introducing electron donor or acceptor atoms or molecules (referred to as n- and p-type doping, respectively) into the hollows of the SWNT lattice [3–15]. When a SWNT sample is exposed to alkali-metal vapours, its resistivity decreases by more than one order of magnitude [3,10–12,15]. The alkali-atoms (n-type doping) are likely inserted in the bundles in between the tubes [5,16,17]. However, possible insertion of the dopant species inside the tube has also been shown in iodine-doped SWNT [6].

Raman spectroscopy is known as one of the most efficient tool to investigate the vibrational properties of SWNT in relation with their structural and electronic properties [18,19]. Raman scattering for SWNT is a resonant process. The resonant behavior of the SWNT Raman spectrum is illustrated by dramatic changes with the excitation energy of the Raman profile of the tangential modes (TM) in the range 1400–1700 cm^{-1}. Fig. 1(a) displays the Raman results for a SWNT sample featured by an average diameter of 1.4 nm and a dispersion of ± 0.2 nm. A broad and asymmetric band around 1540 cm^{-1} and a sharp peak at 1580 cm^{-1} are observed for the 1.92 eV excitation energy (Fig. 1(a), bottom) while several symmetric lines with a dominant peak around 1590 cm^{-1} and two other strong features around 1560 and 1550 cm^{-1} for the 2.41 eV excitation energy (Fig. 1(a), top). The other intense lines observed in the SWNT Raman spectrum appear at lower frequency, typically in the range 100–200 cm^{-1} (not shown), and are associated to the radial breathing modes (RBM) [18,19]. Many experiments and calculations have shown that the RBM frequencies are related to the tube diameters [20,21].

Despite these well established results, the interpretation of Raman first order spectrum is still in debate, and two models based on single-resonance and double-resonance scattering are in discussion. The most conventional approach considers a single-resonance scattering associated with allowed optical transitions (AOT) between spikes in the 1D electronic density of states which fall in the visible and near-infrared ranges for pristine samples. The AOT energies depend both on the diameter and metallic or semiconducting character of the tubes. Therefore, when the excitation energy matches a peculiar AOT energy, the Raman response of the corresponding tube is enhanced. For a tube of diameter 1.4 nm, the single resonance approach predicts the enhancement of the response of the metallic (semiconducting) tubes for the 1.92 eV (2.41 eV) excitation. Interesting is

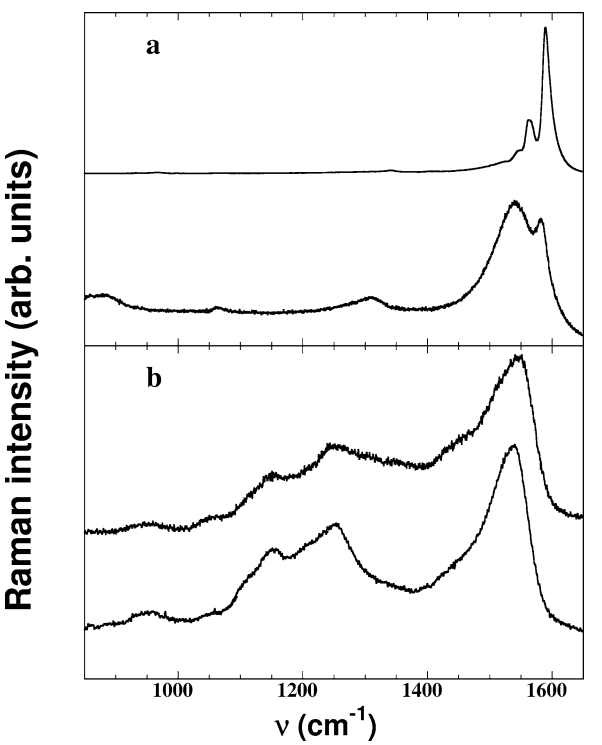

Fig. 1. Raman spectra in the TM range of: (a) pristine SWNT and (b) saturated Rb-doped SWNT bundles at laser excitation energies 2.41 eV (top) and 1.92 eV (bottom).

the profile of the main peak of the Raman response of the metallic tubes excited at 1.92 eV (Fig. 1(a), bottom). It was found that the shape of the lowest frequency dominant component of TM bunch is well described using a Breit–Wigner–Fano (BWF) resonance which involves coupling between a phonon and an electronic continuum [22–25]. It must be pointed out that, in this approach, all modes correspond to Γ-point vibrations. In the second approach, which was proposed more recently, a double resonance process has been put forward to explain the Raman spectrum, and especially the multi-peaks structure of tangential modes [26]. In this approach, some peaks in the TM bunch do not correspond to phonon modes with a wave vector $q \approx 0$ but originate from phonons with a wave vector $q > 0$. This approach well explains the large gap ($\approx$20 cm^{-1}) between the two dominant components of the spectrum centered around 1590 and 1565 cm^{-1} in semiconducting tubes and their positive and negative excitation-energy dependence, respectively.

Because Raman vibrational features are sensitive to both intercalation and charge transfer, this spectroscopy allows us to investigate the evolution of the structural and electronic properties of SWNT upon doping. The first evidence for charge transfer in doped carbon nanotube bundles has been stated in the pioneer work of Rao et al. on saturated K- and Rb-doped SWNT bundles (also on iodine- and Br_2-doped SWNT) [4]. The Raman spectrum of *saturated* alkali-doped SWNT presents the following features: (i) the high frequency tangential modes shift substantially to low frequencies; (ii) the lineshape of the most intense component is well described by a BWF resonance; (iii) new Raman lines are activated in the range 800–1300 cm^{-1}, (iv) RBM vanish. Raman spectroscopy of K-doped SWNT has also been studied using in-situ electrochemical methods [9,10]. It was found that, for stoichiometries corresponding to a K/C atomic ratio above 0.02, the high frequency tangential modes monotonically downshift as a function of the doping level, ΔQ, with: $\Delta\omega/\Delta Q \sim 370$ cm^{-1} per electron per carbon, close to the value obtained in alkali-doped C_{60} ($\Delta\omega/\Delta Q \sim 340$ cm^{-1} per electron per carbon [27]) but larger than the value 280 cm^{-1} per electron per carbon observed in KC_8 graphite [28,29]. In this latter study the most striking result was the observation of an upshift of the tangential modes at low doping level (Fig. 1 of [30]).

It is on the basis of these previous works that we started a Raman study of alkali-doped SWNT bundles. The first objective was to confirm and extend previous results on saturated alkali-doped phases. The second objective was to understand the changes in the Raman spectrum with doping, in relation with: (i) the changes in the electronic properties featured by the enhancement of the conductivity [3,10–12]; and (ii) the changes in the optical absorption spectra featured by a progressive vanishing of peaks associated to van Hove singularities [7,8]. In this aim, Raman experiments were combined with resistivity and/or optical absorption investigations. In Section 2, we present the preparation of alkali-doped samples and the Raman set-up. In Section 3 are reported and discussed the Raman responses in the TM range measured on the saturated phase (Section 3.1), and as a function of the doping level (Section 3.2) (Section 3.2.1: in-situ rubidium vapor phase doping, and Section 3.2.2: Li- and K-doped films of controlled stoichiometry). Conclusions are proposed in Section 4.

2. Doped samples and experimental set-up

All the pristine SWNT samples used in the experiments discussed in this paper were obtained by the arc electric production method [31]. The diameter of nanotubes were found to be distributed from 1.2 to 1.6 nm with various chiralities. Saturated Rb- and Cs-doped SWNT bundles were prepared by vapor phase as described in [17]. The pristine samples were introduced in quartz capillaries, outgassed at 260 °C in vacuum (10^{-5} bars) and then exposed during one day to an excess of alkali-vapor using the classical two bulb method, at $T_{Rb} = 200$ °C and $T_{Cs} = 180$ °C with a small gradient of temperature between alkali-metals and SWNT bundles [17].

To follow the dependence of the Raman spectrum upon doping we have performed combined in situ resistivity and Raman investigations of Rb-doped SWNT bundles. The pristine sample was purified in a four-step method, namely, reflux in nitric acid, dispersion in a surfactant solution, filtration and annealing in vacuum at 1200 °C. The final product was a compact mat, with most of the tubes assembled into crystalline bundles, as shown by diffraction experiments. This kind of sample was doped using the vapor phase method. This method permits to prepare samples at various doping levels. However the stoichiometry of the different samples is not controlled. The reactor was equipped with an optical glass window in order to perform Raman experiments during the doping. A four probe set-up was used to measurements of resistivity [15].

Thin films were obtained by dispersing the pristine material in ethanol and then by spraying on a quartz plate heated with hot air [7]. K- and Li-doped thin films were prepared by redox reactions between SWNT and solutions of different organic radical-anions in pure THF. This method will be called chemical route in the following [7,12]. Optical absorption was used to determine the change in the concentration of radical anions induced by the redox reactions, e.g., the number of electrons transferred from the solution to the sample and therefore the stoichiometry of the sample. For the present work the radical-anions of anthraquinone, benzophenone and naphtalene were used with Li^+ and K^+ as counter-ions leading to $A_{0.04}C$, $A_{0.14}C$ and $A_{0.17}C$ (A = Li, K) stoichiometries [12]. In contrast to the vapor phase procedure, the advantage of the chemical route is to control the stoichiometry. However, it is important to emphasize that the nature of the intercalated species is different than for vapor phase doping. Recently, we confirmed from inelastic neutron scattering experiments that Li^+ and K^+ cations are solvated

by THF molecules during the doping process [32]. Therefore, the inserted species in the doped samples prepared by this route are Li^+ (K^+) cations rounded by several THF molecules, which are labelled: $A^+ + n$THF, with A = Li, K and $1 \leqslant n \leqslant 4$. However, in the following and for facility, the samples will always be labelled A_xC.

Raman spectra were measured using Ar^+–Kr^+ ion laser lines (488 nm, 514.5 nm, 647.1 nm) in the back scattering geometry on a Jobin–Yvon T64000 spectrometer equipped with a liquid nitrogen cooled CCD detector. Room-temperature micro-Raman experiments ($\times 50$ objective) were performed on doped thin films prepared by redox reaction and on saturated samples prepared from the vapor phase route. In-situ macro-Raman experiments were performed during the Rb doping in vapor phase. Additional room temperature spectra excited at 1064 nm were recorded on different samples in a back scattering geometry with a FT Raman Bruker RFS 100 analyser spectrometer. In all these experiments, the average laser power density was kept below 100 W cm^{-2} in order to minimize the local heating.

3. Results and discussion

3.1. Raman response of the saturated alkali-doped phase

Fig. 1 compares the high frequency part of the Raman spectra measured on pristine sample (Fig. 1(a)) and saturated Rb-doped phase (Fig. 1(b)) with laser energies 2.41 eV (514.5 nm) and 1.92 eV (647.1 nm). The spectral profile in the high frequency range is close to that measured by Rao et al. on Rb- and K-doped sample at 2.41 eV. This profile is also close to that measured on Cs-doped phase at this same incident wavelength [33]. To discuss the Raman spectrum of saturated alkali-doped phase, we focus on the results obtained on Rb-doped sample. In contrast with the significant dependence of the Raman spectrum of pristine SWNT bundle with the excitation energy (Fig. 1(a)), the profile of the Raman spectrum of the Rb-doped sample does not change with the excitation energy (Fig. 1(b)). This result is assigned to a loss of the resonance conditions in doped sample. This is in agreement with optical absorption data where peaks attributed to the electronic transitions between pairs of singularities in pristine semiconducting and metallic SWNT vanish upon doping [7,8].

A detailed analysis of the high frequency range for the spectrum excited at 2.41 eV is displayed in Fig. 2. The most intense component is localized around 1557 cm^{-1} and is significantly downshifted in respect to its position in pristine sample. Its profile is broad, asymmetric, systematically associated with a shoulder on its low-frequency side and it is well described by a Breit–Wigner–Fano (BWF) component.

$$I(\omega) = I_0 \frac{[1 + (\omega - \omega_{\mathrm{BWF}})/q\Gamma]^2}{1 + [(\omega - \omega_{\mathrm{BWF}})/\Gamma]^2}, \tag{1}$$

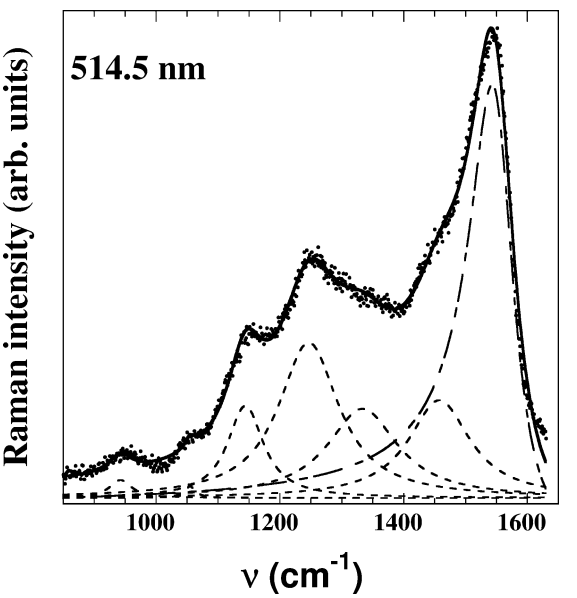

Fig. 2. Typical fit of the TM range for saturated Rb-doped SWNT bundles at laser excitation energies 2.41 eV achieved with a set of 6 lorentzians (dashed lines) and a BWF profile (dot-dashed line).

where $1/q$ is a parameter which measures the interaction of the phonon with a continuum of states, ω_{BWF} is the BWF frequency at maximum intensity I_0 and Γ the broadening parameter.

Similar BWF profile were observed for graphite alkali-intercalated compounds [29] and metallic A_3C_{60} [34]. In pristine SWNT, BWF lineshape is attributed to interference scattering between a plasmon-based electronic continuum and the lower-frequency metallic TM bunch component [25,35]. The negative value of $1/q = -0.36$ that we observe is close to that obtained by Rao et al. [4] (a value around 0.25 was derived in pristine SWNT [22,25]). In contrast with pristine sample, intense bands are evidenced in the 900–1400 cm^{-1} range. All these lines have a Lorentzian lineshape and are tentatively assigned to charge-transfer-softened modes activated by the changes of selection rules in intercalated SWNT bundles. Modelizations of the vibrational dynamics of saturation alkali-doped phase are in progress to precise the attributions of these lines. For the saturated phase, the same Raman responses were observed in Cs-doped sample [33], K-doped sample [4,30,36] and Li-doped sample [30].

In summary, we claim that, from an experimental point of view, the features of the Raman response of saturated alkali-doped phase are now well established. A universal behavior (independent of the alkali metal) of the Raman spectrum of alkali-doped SWNT is found. The Raman response is independent of the excitation energy and the spectra are dominated by a downshifted BWF component. In the following we investigate the dependence of the Raman response with the doping level.

3.2. Dependence of the Raman response as a function of the doping level

3.2.1. Combined in-situ resistivity and Raman studies of Rb doping

To follow the dependence of the Raman spectrum upon doping we performed a combined in situ resistivity and Raman investigations of Rb-doped SWNT bundles.

The resistance curve measured upon doping is displayed in Fig. 3. Specific features can be pointed out. Initially the rubidium is at 150 °C. The resistance monotonically decreases down to a first plateau after 6 hours of doping (point d in Fig. 3). The resistance at the plateau is about 10 times smaller than the initial value. At $t = 10$ hours, the temperature is increased from 150 °C to 200 °C in order to accelerate the reaction. A minimum of resistance is reached at about 12 hours (with a value of about 15 times smaller than the initial value, not shown). Then the resistance slightly increases and stabilizes on a second plateau (point e in Fig. 3) after 22 hours. The same behavior has been measured in several sets of measurements where the temperature was kept constant throughout the whole experiment.

Raman spectra have been continuously measured upon doping. The time dependence of the high frequency part of Raman spectrum excited at 2.41 eV (514.5 nm) and 1.92 eV (647.1 nm) can be observed in Figs. 4 and 5, respectively. The four spectra correspond to points a (pristine sample), b, c and d, respectively, in Fig. 3. Obviously, doping reduces the absolute intensity of the spectrum (Figs. 4 and 5). Focusing on the Raman spectra measured with the 514.5 nm excitation, the most important result is

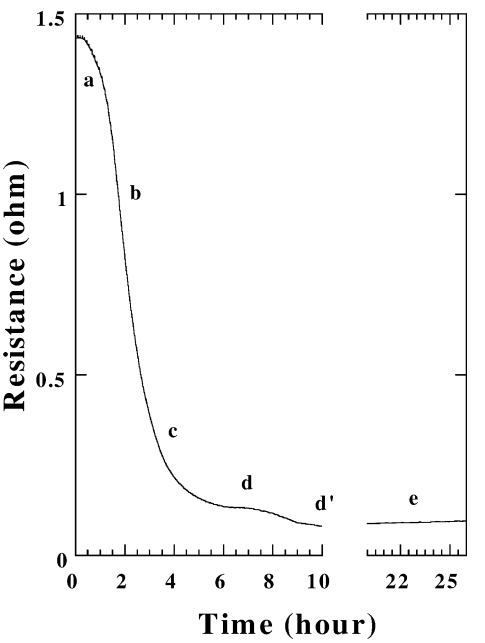

Fig. 3. Evolution of the resistance during the in situ doping experiment.

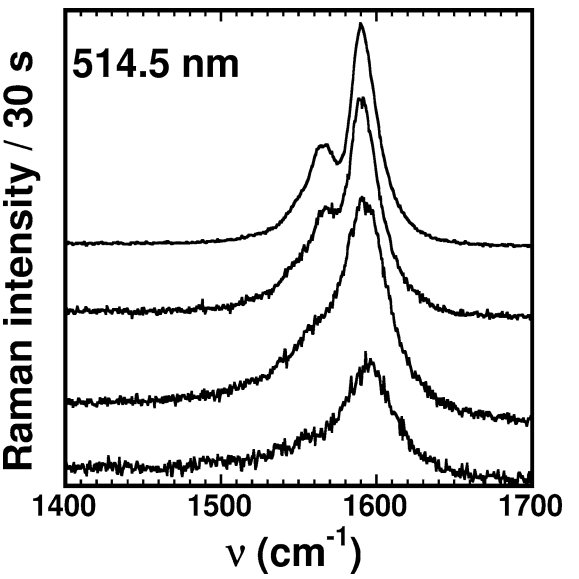

Fig. 4. Evolution of the Raman spectra of the TM excited at 514.5 nm during the in situ doping experiment. From top to bottom, the spectra correspond to different values of the resistance (a, b, c, d), as indicated in Fig. 3.

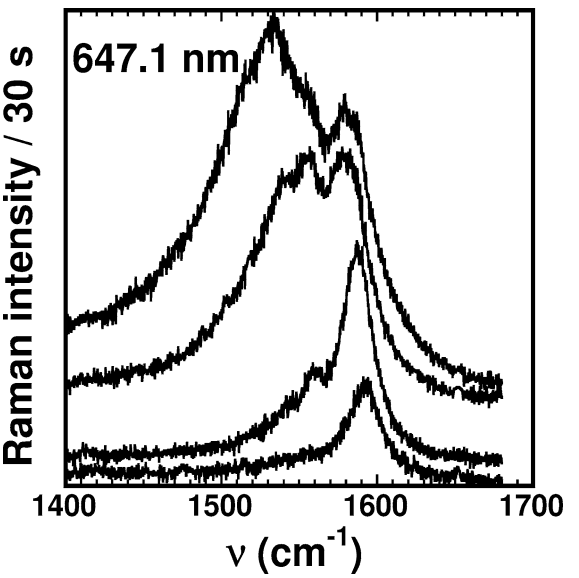

Fig. 5. Evolution of the Raman spectra of the TM excited at 647.1 nm during the in situ doping experiment. From top to bottom, the spectra correspond to different values of the resistance (a, b, c, d), as indicated in Fig. 3.

the evidence of an upshift of the most intense peak of tangential modes (TM) bunch upon doping [15]. This result is in complete opposition with the downshifted spectrum observed in the saturated doped phase [4,33]. A detailed analysis of the dependence of TM upon doping reveals a no significant shift between a and c, by contrast to a progressive (weak) upshift of the main peak from c to d. It can be pointed out that the upshift of TM is in agreement with the previous observation of Claye et al. on K-doped SWNT electrochemically prepared [10,30]. The same behavior of the TM bunch has also been observed for K-doped sample prepared fom vapor phase [36]. We state that this specific behavior is related to the monotonically decrease of the resistance upon doping. The general profile of the tangential modes is also strongly affected by the doping. A monotonous decrease of the intensity of the low-frequency component (around 1570 cm^{-1} in pristine samples) is observed upon doping. At the first plateau of resistance the Raman response is dominated by an *upshifted single component* at 1596 cm^{-1} (bottom spectrum in Fig. 4). More significant is the behavior of the tangential modes in the Raman spectrum excited at 647.1 nm (Fig. 5). In pristine

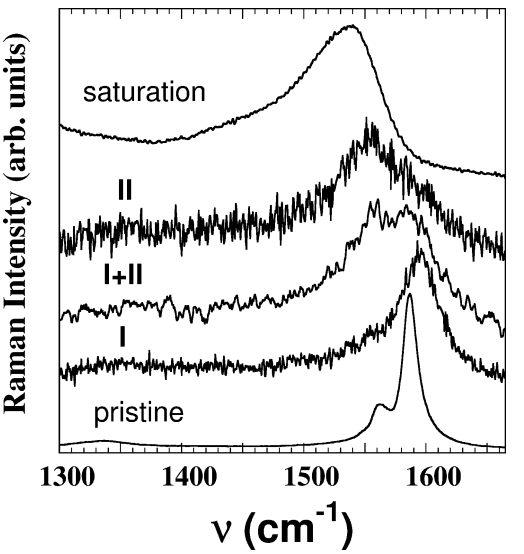

Fig. 6. Comparison between the Raman spectra excited at 2.41 eV for, bottom to top: pristine SWNT, Rb-doped phase I, intermediate Rb-doped (phase I+phase II), Rb-doped phase II (point e), saturated Rb-doped phase [33].

sample this profile is dominated by a low-frequency BWF component assigned to the intrinsic response of metallic tubes. The intensity of this component significantly decreases and its profile is strongly modified upon doping. At points c and d the profile of the Raman spectrum and the peak positions are similar to those observed in the Raman spectrum excited at 514.5 nm. As for the saturated phase, the identity of the Raman responses on the first plateau of resistance for different excitation energies is assigned to the loss of the resonance character of the Raman scattering. In the same experiment, when the second plateau of resistance is reached (point e), a drastic change of the profile of TM is observed (Fig. 6). The Raman spectrum is close to that of the saturated phase (see previous part), namely a downshifted BWF component around 1555 cm^{-1}. However the band at point e is at higher frequency than in the saturated phase (Fig. 6). This result can be related to the monotonic downshift of the BWF component as a function of the doping level, previously observed in [30].

All these results show a specific behavior of the Raman response of the alkali-doped SWNT bundles, slightly dependent on the nature of the alkali-metal, namely a monotonic upshift of the tangential modes related to a monotonic decrease of the resistance upon doping. It is tempting to assign the upshifted single component that dominates the Raman response at the first plateau of the resistance curve to the Raman signature of a specific alkali-doped phase that we label phase I. On the other hand, the downshifted BWF component that appears at high doping level is assigned to the intrinsic Raman response of another alkali-doped phase, phase II. The similarity between the profiles of Raman spectra in phase II and saturated phase suggests that the structure of phase II is similar to that of the saturated phase, only differs the doping level: smaller in phase II than in the saturated phase. The continuous measurements upon doping of the evolution of the spectrum between points d and d′ of the resistance curve allow us to state that the two peaks around 1555 and 1596 cm^{-1} coexist in several spectra, the intensity of the former increasing progressively upon doping to the detriment of that of the latter (Fig. 6). The spectrum d′ is very close to the spectrum e. This result indicates that the two phases coexist in a specific doping range and that the saturated-doped phase, phase II, grows at the expense of phase I.

To measure precisely the dependence of the Raman response with doping we performed experiments on alkali-doped SWNT thin films prepared from chemical route. In this study we correlate the Raman data with optical absorption measurements performed on the same samples.

3.2.2. Combined optical absorption and Raman studies of alkali-doped SWNT

Fig. 7 shows the typical evolution of the optical absorption spectra upon doping in Li_xC films. The main low-energy features in the absorption spectrum of pristine SWNT, located around 0.69, 1.2 and 1.8 eV, are attributed to electronic transitions between pairs of singularities in semiconducting SWNT's (0.69 and 1.2 eV) and first pair of singularity in metallic SWNT's (1.8 eV) [7,8,22]. These features are still observed in $Li_{0.04}C$ film, but the intensity of the lowest energy band is significantly reduced. The same behavior was observed in Cs-doped SWNT films at low doping level [8]. The decrease of these bands in the first stages of doping is explained in terms of the charge-transfer mechanism in the framework of the rigid-band model (progressive filling of the electronic levels of semi-conducting tubes upon doping). All these bands vanish in the $Li_{0.14}C$ and $Li_{0.17}C$ films. The optical absorption of Li_xC films display strong analogies with those of A_xC ($A = Rb, Cs$) samples suggesting that the

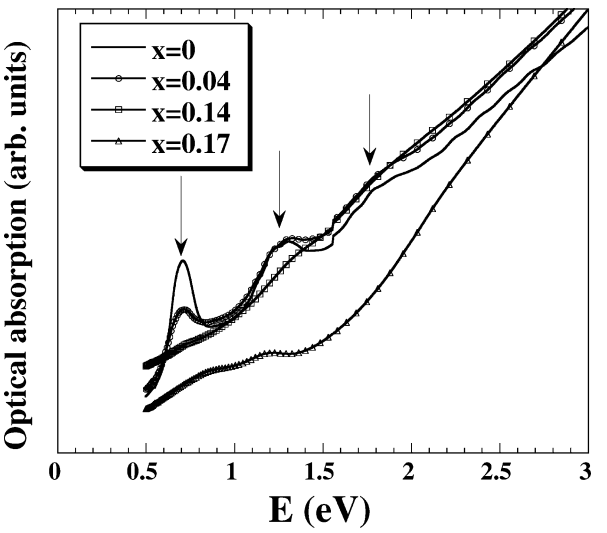

Fig. 7. Evolution of the optical absorption spectra for various stoichiometries: pristine (solid line), $Li_{0.04}C$ (open dots), $Li_{0.14}C$ (open diamonds), $Li_{0.17}C$ (full dots). The optical spectrum of $Li_{0.17}C$ has been shifted for clarity.

properties of alkali-doped SWNT bundles are slightly dependent on the nature of the alkali-metal. Also, the similarity between the optical absorption of Li_xC films and that of vapor phase alkali-doped samples shows a weak sensitivity of the charge transfer to the presence of THF. Optical absorption measurements provide a precise picture of the electronic states in $Li(K)_xC$ films. We have checked that the THF molecules solvating the cations do not affect the optical absorption spectra. Indeed, the optical absorption spectrum of SWNT is not modified by dipping a thin film of nanotubes in pure THF.

The dependence of the Raman response with the stoichiometry in Li_xC films [37] is reported in Fig. 8. Significant changes are observed on the profile of the TM upon doping. For $Li_{0.04}C$ the spectra are close to those measured on pristine samples, especially the resonant character of the Raman response persists in relation with the persistence of the van Hove singularities evidenced in the optical absorption spectrum (Fig. 7). However, as previously observed in the in-situ Raman study of Rb doping, the profile of the lowest frequency component is different from that observed in pristine samples for the 1.92 eV excitation. Its profile is more symmetric and the low-frequency component displays a well defined double-peak structure. In contrast, as expected from their optical absorption spectra, the Raman spectra of $Li_{0.14}C$ and $Li_{0.17}C$ films do not show a resonant character: the profile of the spectra is independent of the wavelength. The highest frequency component dominates the spectrum. The intensity of the components located on the low-frequency side of the main peak (around 1550 and 1567 cm^{-1} in pristine SWNT) decreases with the stoichiometry and this component almost vanishes in $Li_{0.17}C$. These results confirm the behaviors previously found: (i) the most intense component of the TM bunch upshifts when the stoichiometry increases; (ii) the Raman profile is independent of the excitation energy in the highest doped films. Recently this information has been completed by results measured on $K_{0.17}C$ thin films prepared by the same route. In Fig. 9 are compared the profile of the Raman spectrum of $Li_{0.17}C$ and $K_{0.17}C$ thin films for four excitation wavelengths. These profiles are similar in the two samples and independent of the excitation energy.

4. Summary and conclusion

Raman studies performed on samples doped with different alkali metals (Li, K, Rb, Cs) and from different routes (vapor phase, chemical route) allow us to state an universal behavior of the Raman response of alkali-doped SWNT bundles as a function of the doping level, independently of the nature of the alkali metal. In a first step, the profile of TM bunch progressively changes upon doping from a multi-peaks structure to a single upshifted line. This behavior is related to a concomitant monotonic decrease of the resistance and a progressive vanishing of peaks associated to van Hove singularities in optical absorption spectra. In a second step, a drastic change of the Raman profile occurs when the resistance reaches its final stable value. Two distinct Raman responses have been identified in relation with two plateaus in the resistance curve and are assigned to two intrinsic doped phases: *upshifted symmetric single line* associated to phase I (first plateau of resistance) and *downshifted asymmetric BWF component* associated to phase II (second plateau in the resistance curve), structure similar to that of saturated phase at a smaller doping level.

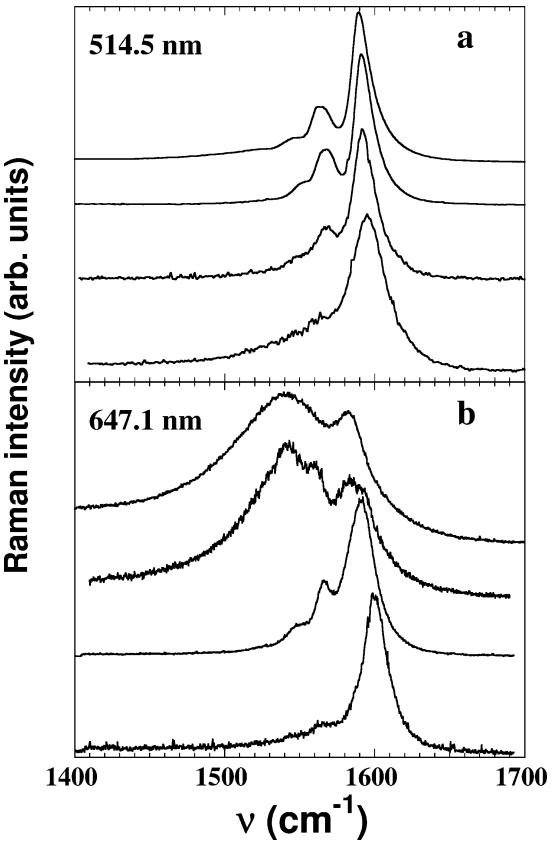

Fig. 8. Raman spectra in the TM range for Li-doped SWNT at various Li/C ratios, (a) excited at 2.41 eV; (b) excited at 1.92 eV. Starting from the top: pristine, $Li_{0.04}C$, $Li_{0.14}C$ and $Li_{0.17}C$.

With regards to the significant difference in the size of the dopant species the strong similarity between the behaviors measured on the different doped samples must be pointed out. This similarity suggests that the observed behaviors relate to the charge transfer for a same localization of the dopant species inside the bundles. To solve the question of the localization of the dopant species combined X-ray and neutron diffraction experiments have been performed and their complete analysis is now in progress [38]. The saturated phase is likely associated to specific organization of the dopant species inside the structure, different of that in phase I. It must be pointed out that the highest chemical composition achieved by the chemical route does not correspond to the saturated phase. This comes from the value of the redox potential of the naphtalene anion radical which is about 0.5 eV smaller than that of alkali metals [7], the chemical composition of the saturated phase being reported in [30] to be close to $Li_{0.21}C$.

To our surprise, some analogies with the behavior of the Raman response upon doping in graphite intercalation compounds can be found [29]: (i) upshifted component at low doping level (stages 2 and 3 in intercalated graphite); (ii) downshifted BWF component at the highest doping level (stage 1 in intercalated graphite). At low doping level, the spectra for alkali-doped graphite exhibit a doublet structure. The intensity of the component close to the frequency of the E_{2g} Raman-active mode for pristine graphite decreases with increasing doping level, while the intensity of the upshifted line increases with increasing doping level [29]. With regards to these behaviors, the lower and upper frequency components are, respectively, identified with vibrations in planes not adjacent to and planes adjacent to an intercalate layer plane. However, in alkali-doped SWNT, an upshift of the highest-frequency component of TM bunch is clearly evidenced and no doublet structure is observed. It must be also pointed out that the shift is weaker than the gap between the components of the doublet in intercalated graphite suggesting weaker interactions between the tubes and the alkali atoms in SWNT than in graphite. The dependence of the Raman spectrum upon doping can be interpreted on the basis of the calculations of the relaxed total energies as a function of the intertube distance for different potassium doping contents [39]. A possible scenario could be: (i) in a first step a progressive and homogeneous intercalation of the bundles by alkali atoms occurs. The hollow channels formed by three tubes seem to be the most convenient sites that allow a monotonic and homogeneous intercalation of alkali atoms inside the bundles, associated to a weak expansion

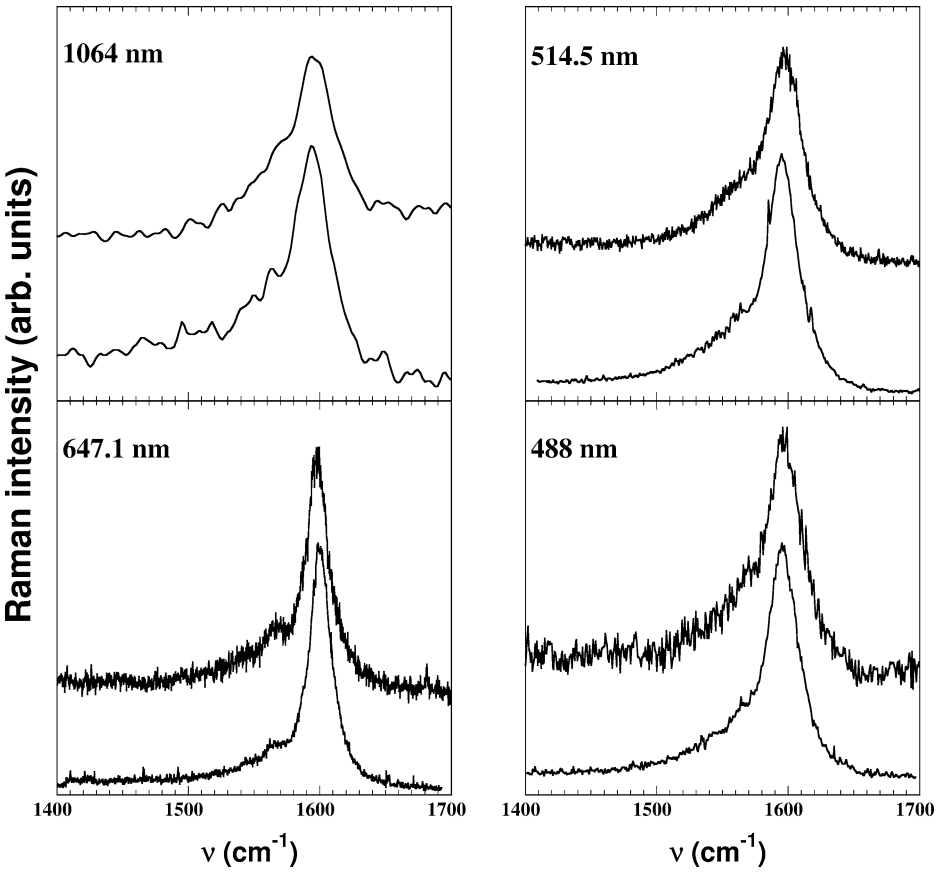

Fig. 9. Comparison between the Raman spectra excited at 1064 nm, 647.1 nm, 514.5 nm and 488 nm, respectively: $K_{0.17}C$ (top curve) and $Li_{0.17}C$ (bottom curve).

of the lattice (for potassium, only 0.4 per cent of lattice expansion is required; 4 per cent of lattice expansion is expected for $A^+ + n$THF dopant) and therefore to a slight shift of TM spectra ((a) to (c) in Fig. 4 and spectrum of $Li_{0.04}C$ in Fig. 8). This first step corresponds to the alkali-doped SWNT lattices displayed in Figs. 1.a and 1.b of [39]. (ii) In a second step the sites between two tubes can be occupied leading to the lattice shown in Fig. 1.c of [39]. These latter sites are comparable to those involved in graphite intercalation compounds (intercalation between two planes). By analogy with graphite, the hardening of the TM component in phase I could be the consequence of the insertion of alkali atoms between tubes (spectrum at point (d) in Fig. 4 and spectrum of $Li_{0.17}C$ in Fig. 8). (iii) In this assumption, phase I could correspond to a saturation phase for alkali atoms localized between tubes and inside channels as shown in Fig. 1(d) of [39]. X-ray diffraction measurements are in progress in order to test this scenario.

In summary, the agreement between the Raman data obtained on various doped samples prepared by different routes and the correlations of the behaviors of the Raman response upon doping with resistivity and optical absorption data support the consistence of our results and unambiguously state the universal character of the stoichiometry dependence of the Raman spectrum in alkali-doped SWNT bundles.

Acknowledgements

We thank R. Almairac, J.-L. Bantignies, P. Poncharal, S. Rols and A. Zahab from the Groupe de Dynamique des Phases Condensées de Montpellier for usuful discussions. Saturated Rb-doped samples were provided by L. Duclaux from the Centre de Recherche de la Matière Divisée d'Orleans. Li- and K-doped SWNT thin films were provided by C. Mathis and R. Klement from Institut Charles Sadron de Strasbourg. We are grateful to S. Lefrant and J.-Y. Mevellec from the Institut des Matériaux de Nantes for their help in the Fourier-Transform Raman experiments.

References

[1] W. Andreoni (Ed.), The Physics of Fullerene Based and Fullerene-Related Materials, Kluwer Academic, Dordrecht, 2000.
[2] A. Thess, R. Lee, P. Nikolaev, H. Dai, P. Petit, J. Robert, C. Xu, Y. Hee, S.G. Kim, A.G. Rinzler, D.T. Colbert, G.E. Scuseria, D. Tománek, J.E. Fischer, R. Smalley, Science 273 (1996) 483.
[3] R.S. Lee, H.J. Kim, J.E. Fischer, A. Thess, R.E. Smalley, Nature 388 (1997) 255.
[4] A.M. Rao, P.C. Eklund, S. Bandow, A. Thess, R.E. Smalley, Nature 388 (1997) 257.
[5] C. Bower, S. Suzuki, K. Tanigaki, O. Zhou, Appl. Phys. A 67 (1998) 47.
[6] L. Grigorian, G.U. Sumanasekera, A.L. Loper, S. Fang, J.L. Allen, P.C. Eklund, Phys. Rev. B 58 (1998) R4195.
[7] P. Petit, C. Mathis, C. Journet, P. Bernier, Chem. Phys. Lett. 305 (1999) 370.
[8] S. Kazaoui, N. Minami, R. Jacquemin, H. Kataura, Y. Achiba, Phys. Rev. B 60 (1999) 13339.
[9] A. Claye, J.E. Fischer, Electrochim. Acta 45 (1999) 107.
[10] A. Claye, N.M. Nemes, A. Jánossy, J.E. Fischer, Phys. Rev. B 62 (2000) R4845.
[11] B. Ruzicka, L. Degiorgi, R. Gaal, L. Thien-Nga, R. Bacsa, J.-P. Salvetat, L. Forró, Phys. Rev. B 62 (2000) 4845.
[12] E. Jouguelet, C. Mathis, P. Petit, Chem. Phys. Lett. 318 (2000) 561.
[13] R.S. Lee, H.J. Kim, J.E. Fischer, J. Lefebvre, M. Radosavljevic, J. Hone, A.T. Johnson, Phys. Rev. B 61 (2000) 4526.
[14] M. Bockrath, J. Hone, A. Zettl, P.L. Mac Euen, A.G. Rinzler, R.E. Smalley, Phys. Rev. B 61 (2000) R10606.
[15] N. Bendiab, L. Spina, A. Zahab, P. Poncharal, C. Marliere, J.-L. Bantignies, E. Anglaret, J.-L. Sauvajol, Phys. Rev. B 63 (2001) 153407.
[16] G. Gao, T. Cagin, W.A. Goddar III, Phys. Rev. Lett. 80 (1998) 5556.
[17] L. Duclaux, K. Metenier, J.P. Salvetat, P. Lauginie, S. Bonnamy, F. Béguin, Mol. Cryst. Liq. Cryst. 34 (2000) 769.
[18] M.S. Dresselhaus, P.C. Eklund, Adv. in Phys. 49 (2000) 705, and references therein.
[19] J.-L. Sauvajol, S. Rols, E. Anglaret, L. Alvarez, Carbon 40 (2001) 1697.
[20] S. Rols, A. Righi, L. Alvarez, E. Anglaret, R. Almairac, C. Journet, P. Bernier, J.-L. Sauvajol, A.M. Benito, W.K. Maser, E. Muñoz, M.T. Martinez, G.F. de la Fuente, A. Girard, J.-C. Ameline, Eur. Phys. J. B 18 (2000) 201, and references therein.
[21] L. Henrard, V.N. Popov, A. Rubio, Phys. Rev. B 64 (2001) 205403.
[22] H. Kataura, Y. Kumazawa, Y. Maniwa, I. Umezu, S. Suzuki, Y. Ohtsuka, Y. Achiba, Synth. Metals 103 (1999) 2555.
[23] M.A. Pimenta, A. Marucci, S.A. Empedocles, M.G. Bawendi, E.B. Hanlon, A.M. Rao, P.C. Eklund, R.E. Smalley, G. Dresselhaus, M.S. Dresselhaus, Phys. Rev. B 58 (1998) R16016.
[24] L. Alvarez, A. Righi, T. Guillard, S. Rols, E. Anglaret, D. Laplaze, J.-L. Sauvajol, Chem. Phys. Lett. 316 (2000) 186.
[25] S.D.M. Brown, A. Jorio, P. Corio, M.S. Dresselhaus, G. Dresselhaus, R. Saito, K. Kneipp, Phys. Rev. B 63 (2001) 155414.
[26] J. Maultzsch, S. Reich, C. Thomsen, Phys. Rev. B 65 (2002) 33402.
[27] H. Kuzmany, M. Matus, B. Burger, J. Winter, Adv. Mater. 6 (1994) 731.
[28] P.C. Eklund, G. Dresselhaus, M.S. Dresselhaus, J.E. Fischer, Phys. Rev. B 16 (1977) 3330.
[29] M.S. Dresselhaus, G. Dresselhaus, Adv. in Phys. 30 (1981) 139.
[30] A. Claye, S. Rahman, J.E. Fischer, A. Sirenko, G.U. Sumanasekera, P.C. Eklund, Chem. Phys. Lett. 333 (2001) 16.
[31] C. Journet, W.K. Maser, P. Bernier, A. Loiseau, M. Lamy de la Chapelle, S. Lefrant, P. Deniard, R. Lee, J.E. Fischer, Nature 388 (1997) 756.
[32] N. Bendiab, R. Almairac, S. Rols, J.-L. Sauvajol, P. Petit, in press.
[33] N. Bendiab, A. Righi, E. Anglaret, J.-L. Sauvajol, L. Duclaux, F. Beguin, Chem. Phys. Lett. 339 (2000) 305.
[34] P. Zhou, K.A. Wang, P.C. Eklund, M.S. Dresselhaus, G. Dresselhaus, Phys. Rev. B 48 (1993) 8142.
[35] K. Kempa, Phys. Rev. B 66 (2002) 195406.
[36] Y. Iwasa, H. Fudo, Y. Yatsu, T. Mitani, H. Kataura, Y. Achiba, Synth. Met. 121 (2001) 1203.
[37] N. Bendiab, E. Anglaret, J.-L. Bantignies, A. Zahab, J.-L. Sauvajol, P. Petit, C. Mathis, S. Lefrant, Phys. Rev. B 64 (2001) 245424.
[38] R. Almairac, in press.
[39] C. Jo, C. Kim, Y.H. Lee, Phys. Rev. B 65 (2002) 35420.